

Interaction of Bovine Serum Albumin with Chrysotile: Spectroscopic and Morphological Studies

Giuseppe Falini,^[a, b] Elisabetta Foresti,^[b] Isidoro G. Lesci,^[b] Bruno Lunelli,^[b] Piera Sabatino,^[b] and Norberto Roveri*^[b]

Abstract: The biodurability of chrysotile fibers, which is related to their cytotoxicity and mutagenic responses, is strongly affected by the surface chemical adsorption of biological molecules. Natural chrysotile is a heterogeneous material in both structure and composition. The availability of synthetic stoichiometric chrysotile of constant structure and uniform morphology has allowed us to investigate its interaction with bovine serum albumin (BSA). By using transmission electron microscopy

(TEM) and atomic force microscopy (AFM), we have obtained the first morphological evidence of albumin adsorption onto chrysotile nanocrystals. FTIR spectroscopy was used to quantify modifications of BSA secondary structure that were induced by the surface interaction. The protein transition

to β -turns allows a stronger interaction between the protein hydrophilic side-chains and the charged asbestos surface, which is consistent with hydrogen bonds involving the superficial OH groups. Synthetic stoichiometric chrysotile nanocrystals were shown to be an ideal reference standard with which to study the interaction of asbestos fibers with biological systems, in order to elucidate the chemical mechanisms of asbestos toxicity.

Keywords: adsorption • asbestos • chrysotile • nanocrystals • protein modifications

Introduction

Chrysotile is the main form of asbestos, the commercial term referring to a group of fibrous silicates with high tensile strength, fire and heat resistance, chemical inertia, and electrical resistivity. Because of these properties, chrysotile fibers have been widely utilized for many industrial applications and account for approximately 95% of manufactured asbestos.^[1]

The layered structure of chrysotile, $(\text{Mg}_3\text{Si}_2\text{O}_5(\text{OH})_4)_n$, consists of linked $(\text{Si}_2\text{O}_5)_n^{2-}$ sheets inserted between brucite-type octahedral layers. On one side, two from every three hydroxyl groups are replaced by apical oxygen of the tetrahedral silica. The sheets of tetrahedral silica have a lateral dimension smaller than that of the magnesium hydroxide octahedral sheets, resulting in a structural mismatch that is

fully compensated by the curvature of the layers. The structure of single crystals of chrysotile is thus characterized by tetrahedral and octahedral layers curled concentrically or spirally, usually around the x axis (orthochrysotile) and seldom around the y axis (parachrysotile), into a tubular structure of about 20–50 nm in diameter. The rolls possess hollow cores with a diameter of about 7–8 nm, because the layers cannot withstand a curvature that is too tight.^[2]

Mineral chrysotile fibers show different structures (conical, cone-in-cone, cylinder-in-cylinder, polygonal, and spirally concentric tube), depending on the ore growth conditions, which probably differ according to the mineral source location. The chrysotile morphologies and structures have been widely investigated by using X-ray diffraction,^[3] electron microscopy and electron diffraction.^[4] Isomorphic substitutions of Mg and Si cations are favored and occur frequently; therefore, variable stoichiometry is characteristic of the natural chrysotile.^[5,6]

Stoichiometric single nanocrystals of chrysotile were recently synthesized as a unique phase with definite structure, morphology, and chemical composition. They consist of nanocrystals showing single-cylinder and two-cylinders morphology, with a central hole diameter of 7 ± 1 nm and an outer diameter of 20 ± 2 nm (single cylinder) and 50 ± 3 nm (two cylinders).^[7,8] These chrysotile nanocrystals may be

[a] Dr. G. Falini
Environmental Chemistry Laboratory, University of Bologna
via dell'Agricoltura 5, 48100 Ravenna (Italy)

[b] Dr. G. Falini, Prof. E. Foresti, Dr. I. G. Lesci, Prof. B. Lunelli,
Prof. P. Sabatino, Prof. N. Roveri
Department of Chemistry "G. Ciamician", Alma Mater Studiorum
University of Bologna, via Selmi 2, 40126 Bologna (Italy)
Fax: (+39)051-209-9593
E-mail: norberto.roveri@unibo.it

used as a standard for the study of their physicochemical properties and interaction with biological systems.

The health hazards associated with asbestos are well documented and its deleterious environmental effects are well known.^[9] Unfortunately, the mechanisms that link exposure to asbestos fibers and the subsequent development of fibrogenesis (asbestosis) and carcinogenesis (bronchogenic carcinoma and mesothelioma) are largely unknown. Several investigations have indicated that asbestos toxicity may be related to the production of reactive oxygen species (ROS) and other free-radical species, and genetic factors may predispose the development of pathologies.^[10,11] The capability of asbestos fibers to enhance ROS production depends on two features of the fibers; their chemistry and their morphology.^[12–14] The physicochemical properties of asbestos fibers are also responsible for their solubility, biodegradability, and biopersistence.^[15] The fibers' properties that are related to their cytotoxicity^[16,17] and mutagenic responses^[18] are strongly affected by the surface chemical adsorption of biological molecules and macromolecules, such as proteins, cell-membrane lipids, and nucleic acids.^[12] Alterations in these essential cellular components can alter cell functions and hence drive the cell to either neoplastic transformation or apoptosis. The adsorption of serum macromolecules, such as fibronectin and albumin, onto mineral asbestos fibers has been studied to obtain information about the phagocytosis and toxicity of asbestos fibers for mesothelial cells.^[19] Albumin, the major plasma protein, is a highly soluble protein that can be prepared at concentrations of up to 30% (w/v).^[20] This property is related to its negative charge at neutral pH. The amino acid sequence of albumin is characterized by unusually high percentages of cysteine (35) and charged amino acids, and low percentages of tryptophan, glycine, and methionine.^[21,22] Additionally, and unusually for extracellular proteins, it possesses a single, free sulfhydryl (Cys 34) and has no sites for enzymatic glycosylation.^[21,23] The crystalline human serum albumin (HSA) structure is predominantly α -helical, with the remaining polypeptide existing in turns and extended or flexible regions between subdomains.^[24] The heart-shaped HSA molecule is made up of three homologous domains (I, II, III).^[25] Each domain contains two subdomains (A and B) that share common structural motifs, and each of these can be divided into ten helical segments.

The three-dimensional structure of bovine serum albumin (BSA) is believed to be very similar to that of HSA; the two proteins share 76% sequence identity. The most important compositional difference is the presence of more tryptophanes in BSA.^[26] Results of FTIR investigations of BSA secondary structures revealed a significant difference between the aqueous and lyophilized states. In fact, lyophilization of proteins generally causes a decrease in α -helix content and an increase in β -sheet content. The latter is due to protein–protein interactions that lead to the formation of intermolecular β -sheets if water is removed.^[27a,b] Indeed, according to the authors, BSA in aqueous solution at pH 7.4 shows an α -helix content of $54 \pm 6\%$, whereas lyophilized

BSA has an α -helix content of $31 \pm 3\%$; β -sheet content is about $8 \pm 3\%$ in aqueous BSA versus $22 \pm 3\%$ in lyophilized BSA. The remaining secondary structures are present at $38 \pm 1\%$ in solution and $47 \pm 3\%$ in the lyophilized powder.

Morgan has studied the adsorption of HSA onto various mineral asbestos fibers and showed that adsorption involves only the external surface of the fiber and the equilibrium between protein in solution and adsorbed protein is reached within a few minutes.^[28] In the last decades, the adsorption of albumin onto mineral asbestos fibers has been investigated by employing X-ray photoelectron spectroscopy (XPS),^[29] FTIR and NMR spectrometries,^[30] revealing the tendency of mineral chrysotile fibers to yield adducts with albumin. These studies have dealt mainly with electrostatic interactions between the asbestos surface and albumin, focusing on the different behaviors of chrysotile and crocidolite. No modification induced in the albumin structure by the interaction with chrysotile fibers has been reported previously. In addition, the results of these studies are strongly affected by the structural and compositional heterogeneity of the mineral chrysotile fibers and by the organic solvents employed. The current availability of a synthetic standard chrysotile provides a tool with which accurate studies of the chrysotile–albumin surface interaction can be performed. In this paper, we investigate the interaction of BSA with mineral and synthetic chrysotile fibers by using FTIR, transmission electron microscopy (TEM), and atomic force microscopy (AFM) techniques, and show the first morphological evidence of albumin adsorption onto chrysotile nanocrystals. This allows us to quantitatively evaluate the protein secondary-structure modifications induced by the electron-donor sites present on the surface of synthetic chrysotile nanocrystals, which act as a reliable reference standard sample.

Experimental Section

Chemical reagents: Reagents were from Sigma–Aldrich, 0.06 M phosphate buffer pH 7.4 was from Riedel-de Haen Sigma–Aldrich, and BSA was from Merck.

Mineral chrysotile fibers: UICC (Union Internationale Contre le Cancer) A (Rhodesian) chrysotile fibers were used.

Synthesis of stoichiometric chrysotile nanocrystals: Stoichiometric chrysotile fibers were synthesized as a unique phase by means of hydrothermal reactions under controlled conditions.^[7] MCM41 (average pore size of 3.9 nm and a specific surface area of $910 \text{ m}^2 \text{ g}^{-1}$) was used as a silica source,^[8] instead of the reported silica gel, to satisfy the required purity of the reactants in terms of metal ions. The reaction was performed by mixing MCM41 in 0.1 M aqueous MgCl_2 solution; the Si/Mg molar ratio was 0.68. The pH was raised to 13.0 by adding 1 M NaOH solution, then hydrothermal treatment at 82 atm and 300°C for 24 h was performed. These reaction conditions allowed us to obtain chrysotile nanocrystals as a unique stoichiometric phase with constant structure, crystallinity, sizes, morphology, and surface area.^[8]

Preliminary treatment of chrysotile fibers: The natural chrysotile sample was ground in a mechanical mortar (IKA, model A10) for 30 min at 150 rpm, before its characterization and use. Following mechanical grinding, the fibers partially disaggregate to give a mixture of small fibers and their constituent nanocrystals. Aqueous suspensions (50 mg/30 mL) of the

natural and synthetic chrysotile mixtures were ultrasonicated (model ultrasonic UTA, Falc) for 20 and 2 min, respectively.

Chrysotile–albumin adduct preparation: A sample (20 mg) of mineral or synthetic chrysotile was suspended in 0.06 M phosphate buffer (25.5 mL, pH 7.4) at 37°C. To obtain the chrysotile–albumin adduct, 0.06 M phosphate buffer (4.5 mL, pH 7.4) containing 0.45 μM BSA was added to the above mixtures. All the suspensions, with or without added albumin, were stirred in a water bath at 37°C for 2 h. Successively, the samples were filtered through nitrocellulose filter (pore diameter 0.8 μm), repeatedly washed with deionized water, and then air dried at 37°C.

FTIR analysis: Prior to taking FTIR measurements, the samples were lyophilized from the buffer solution. The infrared spectra were measured from 4000 to 400 cm^{-1} with 2 cm^{-1} resolution by using a Bruker IFS 66v/S spectrometer. The sample-compartment atmosphere had a total pressure of 2 mbar of air, dried to an atmospheric dew point of -40°C ($p_{\text{H}_2\text{O}} \approx 13$ Pa) by means of a Balston 76–01 Membrane Air Dryer. Other settings include an 8 mm aperture, 16 scans, velocity 10 kHz, DLATGS detector, and a 3-term Blackman–Harris apodization function. KBr pellets were obtained under vacuum by using 2 mg of the powdered samples carefully mixed with 200 mg of infrared-grade KBr.

Fourier self-deconvolution and second-derivative resolution enhancement were applied to narrow the widths of the infrared bands and to increase the separation of the overlapping components. The resolution enhancement resulting from self-deconvolution and the second derivative is such that the number and position of the component bands to be fitted are determined. The curve-fitting was carried out by employing BRUKER OPUS peak software (version 4.0). The number of bands was entered into the program along with their respective positions and half-heights. The program iterates the curve-fitting process to achieve the best Gaussian-shaped curves that fit the protein spectrum. A best fit is determined by the root mean square (rms) of differences between the original protein spectrum and the sum of all individually resolved bands. The component bands in amide I and amide III of BSA were assigned according to the literature data. The percentages of each secondary structure were calculated from the integrated areas of the component bands in amide I and amide III, respectively.

TEM images were obtained by using a Philips TEM CM100. Samples were suspended in doubly distilled water and sonicated for two minutes to disaggregate the particles, without any additional treatment. A drop of the chrysotile suspension was transferred onto porous carbon foils supported on conventional copper microgrids. Samples for AFM were prepared by adsorbing a diluted water suspension of chrysotile (1 mg per 10 mL) onto freshly cleaved mica at room temperature for 10 min. The mica surface was then thoroughly rinsed with doubly distilled water and dried under N_2 flow. For AFM imaging, a Digital Instruments Nanoscope IIIa Multimode SPM was used. The samples were imaged in contact mode by using a J scanner and silicon nitride tips (200 μm long with nominal spring constant 0.06 N m^{-1}). The images were flattened offline.

Measurement of specific surface area: Specific surface area was determined by N_2 adsorption at 77 K, by using an automatic gas-volumetric apparatus (ASAP 2010, Micromeritics), and adopting the well-known BET method.^[31]

Results and Discussion

Morphological observations were made on natural and synthetic chrysotile fibers. The latter were prepared as a stoichiometric unique phase by performing a hydrothermal reaction under controlled conditions (see Experimental Section). The natural chrysotile used was the UICC A standard sample. Prior to making the morphological observations, the samples were ground and sonicated to disaggregate the fibers into smaller fibers and their constituent nanocrystals. The samples obtained are hereafter referred to as chrysotile fibers.

Figure 1a and b show images of the synthetic chrysotile fibers, obtained by using AFM and TEM, respectively. The nanocrystals display single-cylinder and two-cylinders morphologies, with a central hole diameter of 7 ± 1 nm and an

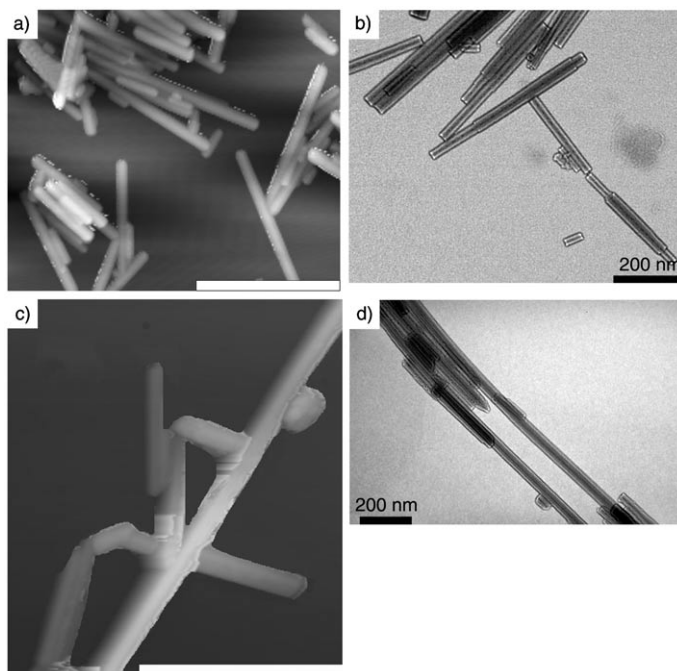


Figure 1. Morphological comparison between natural and synthetic chrysotile crystals. a) and c): AFM images of synthetic and natural chrysotile, respectively. b) and d): TEM images of synthetic and natural chrysotile, respectively. In a) and c) the scale bar represents 1 μm .

outer diameter of 20 ± 2 (single cylinder) and 50 ± 3 nm (two cylinders). Crystals with “cylinder-in-cylinder” morphology consist of two concentric layers that, however, do not extend over the full length of the tube, thereby leading to a step in the outer wall. However, in natural chrysotile crystals in which the two-cylinders morphology is the most common, such steps are rare.^[8]

Figure 1c and d show images of natural chrysotile, obtained by using AFM and TEM, respectively. The fibers are composed of single, tubular crystals and exhibit a wide range in diameter, from 20 to 100 nm, suggesting the presence of several concentric cylinders. However, the majority of fibers have diameters similar to those of synthetic fibers. The morphology of the natural fibers is quite variable and, together with the cylinder-in-cylinder form, other types of morphologies, such as cone-capped and cone-in-cone, are observed. In Figure 1d, one example of a cone-capped crystal is shown. Its uniformity in morphology and size clearly distinguish the synthetic chrysotile from the natural chrysotile.

The surface area of synthetic chrysotile fibers, measured by using the BET method,^[31] is $55 \text{ m}^2 \text{ g}^{-1}$, which is twice that

of natural UICC A fibers (ca. $27 \text{ m}^2 \text{ g}^{-1}$).^[32] It is well known that the surface area is strictly related to the fiber dimensions. The samples were ground and sonicated before BET measurements were taken. The natural chrysotile fibers are larger than the synthetic fibers, and a lengthy disaggregation treatment would be necessary to reduce their average size to that of the synthetic fibers. However, such treatment induces significant changes in the degree of crystallinity and surface properties of the mineral fibers.^[33] Because this study concerns investigation of the surface interaction between chrysotile fibers and serum albumin, we chose to use different surface areas in the natural and synthetic samples instead of introducing modifications in the surface structure.

Chrysotile–albumin adducts were prepared by an optimized procedure in which pH and temperature were chosen close to physiological values to reduce protein denaturation and enable data of the highest biological relevance to be obtained. Under the same experimental conditions (pH 7.4 and 37°C), it was found that 1 g of natural chrysotile was able to adsorb about 3 mg of albumin, whereas 1 g of synthetic chrysotile adsorbed about 30 mg of albumin. The amount of linked albumin was determined by using the spectrophotometric method. The result obtained is very close to that observed by Valerio et al., who used samples of natural chrysotile treated with ultrasound and a different analytical method.^[34] The difference in the amounts of albumin adsorbed onto synthetic and natural chrysotile is related to the different surface area of the fibers, and hence expected. In addition, the amount of albumin adsorbed per unit area of chrysotile is notably higher for the synthetic (600 ng per m^2) than for the natural (100 ng per m^2) sample, although this could be partially related to the different accessibility of the surfaces.

The interaction between chrysotile and albumin was allowed to take place at pH 7.4, at which point albumin (z potential = 5.8) and chrysotile (z potential = 9.2) are predominantly negatively and positively charged, respectively. Thus, an electrostatic interaction should facilitate the adhesion between albumin and chrysotile. However, the stability of this interaction might be governed by other chemical interactions, such as hydrogen bonds.

Chrysotile–albumin adducts were characterized first morphologically, and then by infrared spectra. In the AFM and TEM images obtained from synthetic chrysotile–BSA adducts, the BSA coverage of the chrysotile nanocrystals can be observed. The AFM image (Figure 2a) shows an aggregate of synthetic chrysotile nanocrystals. The protein acts as glue among the nanocrystals and induces fibers aggregation. In the TEM images (Figure 2b), some isolated chrysotile–albumin adducts are shown. The thickness of the dry protein layer on the crystal surface is not uniform and varies even within the same crystal. This indicates that several protein layers are deposited onto the crystal surface; in addition, the protein evidently bridges single nanocrystals. Figure 2c and d show TEM and AFM images, respectively, of the natural chrysotile–albumin adducts. These adducts are characterized by a large variability in protein mineral coverage

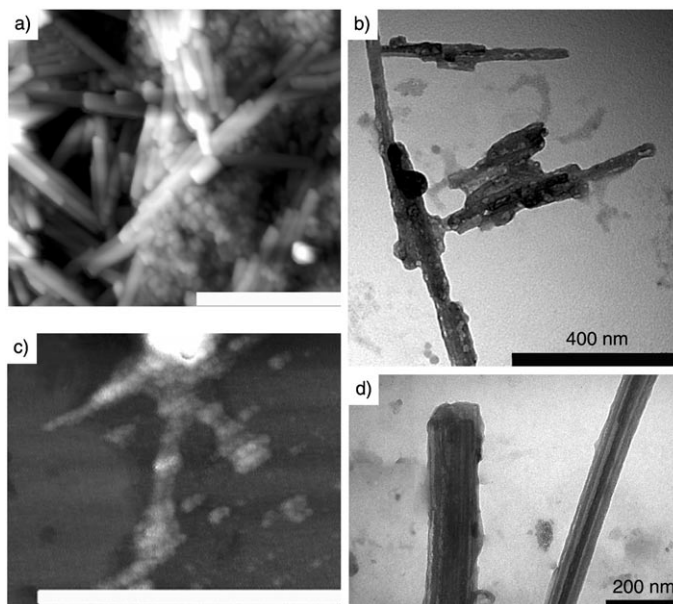


Figure 2. Morphological comparison between natural and synthetic chrysotile–BSA adducts. a) and c): AFM images of synthetic and natural chrysotile–BSA adducts, respectively. b) and d): TEM images of synthetic and natural chrysotile–BSA adducts, respectively. In a) and d) the scale bar represents $1 \mu\text{m}$.

and protein mineral aggregation properties; this could be due to the characteristically heterogeneous morphology and composition of the mineral fibers.

FTIR spectra obtained from natural and synthetic chrysotile samples revealed only limited differences in their characteristic absorption bands. In the natural chrysotile FTIR spectrum, a general band-broadening, related to low crystallinity, and a minimal band-shift, due to the presence of trace amounts of foreign ions, were observed.^[8,35] Because the natural chrysotile presents extensive morphological heterogeneity and the different samples differ drastically in crystallinity and the presence of foreign ions, the structural changes associated with the interface interaction between albumin and chrysotile were studied by using nanocrystals of stoichiometric synthetic chrysotile.^[7,8]

The FTIR spectra of synthetic chrysotile, BSA, and the adduct chrysotile–BSA were compared within the range $4000\text{--}400 \text{ cm}^{-1}$. The assignments of the adsorption bands of the chrysotile, the lyophilized BSA, and the lyophilized chrysotile–BSA adduct are reported in Table 1. The absorption bands of chrysotile and BSA are in agreement with those from literature data.^[36a–c] In the FTIR spectrum recorded for the chrysotile–BSA adduct, all the characteristic chrysotile and protein FTIR absorption bands are present, however, band-shift and absorption-intensity changes are observed.

Figure 3a and b show the FTIR spectra of the chrysotile and the chrysotile–BSA adduct, respectively, within the range $1200\text{--}400 \text{ cm}^{-1}$. Differences between the chrysotile and the adduct were observed: the shift of the absorption band at 1080 cm^{-1} to 1085 cm^{-1} , attributed to the out-of-

Table 1. Assignment of the FTIR adsorption bands of chrysotile, BSA, and the chrysotile–BSA adduct.

FTIR band [cm ⁻¹]	Chrysotile		Adduct		Bovine serum albumin	
	assignment	FTIR bands from chrysotile [cm ⁻¹]	FTIR bands from BSA [cm ⁻¹]	FTIR band [cm ⁻¹]	assignment	
3694	in-phase outer Mg–OH stretch	3694	3200–3400	3200–3400	N–H stretch	
3646	in-phase inner Mg–OH stretch	3647	3065	3056	C–H stretch	
3694 (shoulder)						
1080	out-of-plane symmetric $\nu(\text{Si–O})$ vibration	1085	2961 w ^[a]	2959	CH ₃ asymmetric stretch	
1015	$\nu(\text{Si–O})$ vibration in plane parallel to the <i>b</i> axis	1015	2926 s ^[a]	2928	CH ₂ asymmetric stretch	
959	$\nu(\text{Si–O})$ vibration in plane parallel to the <i>a</i> axis	959	2872 w ^[a]	2871	CH ₃ symmetric stretch	
649	outer Mg–OH libration	649	2854 s ^[a]	2854	CH ₂ symmetric stretch	
607	inner Mg–O libration	605	1657 s ^[a]	1653	amide I	
584	antisymmetric vibration mode of the Mg–O group	582 w ^[a]	1554 w ^[a]	1539	amide II	
557	perpendicular Mg–O/Si–O bend	557	1457 s ^[a]	1455	CH ₂ bend	
484	Mg–OH translation vibration	471 w ^[a]	1384 w ^[a]	1385	CH ₃ rocking	
438	Si–O–Mg bend	435	1407	1394	$\nu(\text{COO})_{\text{sym}}$	
			1311–1271 w ^[a]	1303–1242	amide III	

[a] w and s indicate that the peak intensity is relatively weaker or stronger, respectively, than that of the pure BSA.

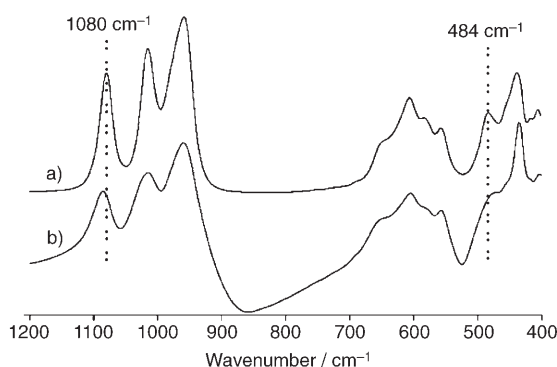


Figure 3. FTIR spectra obtained from ground samples (tens of micrograms) in KBr pellets of a) synthetic chrysotile and b) synthetic chrysotile–BSA adduct. The spectra were collected within the range 1200–400 cm⁻¹. The absorbance is in arbitrary units.

plane symmetric $\nu(\text{Si–O})$ vibration, and the shift of the absorption band at 484 cm⁻¹ to 471 cm⁻¹, attributed to the chrysotile outer Mg–OH vibration. Consistent with this variation, the Mg–O vibration modes at 607 cm⁻¹ and 584 cm⁻¹ are also shifted slightly to lower wavenumbers. These data indicate an interaction between the protein and the chrysotile OH groups of the surface brucite layer. Therefore, the observed shift of Si–O vibration bands following albumin adsorption may indicate that albumin is also entering the hollow core of the crystal. In fact, the tetrahedral layer is exposed to the solution only in the interior of the tube and at the edges.

The conformational changes in the protein induced by adsorption onto the chrysotile surface were evaluated by using FTIR spectroscopy. An evaluation of the percentage content of each secondary structure was carried out based on a range for each conformation defined according to literature data.^[37–41] The spectral data for both the amide I and amide III regions were analyzed to validate the band assignments by using two different spectral regions. Figure 4 shows the original and curve-fitted FTIR spectra of the amide I and amide III bands before and after the interaction of protein

with chrysotile. Analysis of the FTIR spectra of free lyophilized BSA by Gaussian curve-fitting revealed an α -helix content of 31 ± 1% for the amide I region and 31 ± 2% for the amide III region. The content of β -sheet structure is 22 ± 1% for the amide I region and 24 ± 3% for the amide III region. In addition, the content of random structure is 22 ± 3% for the amide I region and 24 ± 2% for the amide III region. Finally, free BSA shows a β -turn content of 24 ± 1% for the amide I region and 20 ± 3% for the amide III region. We also determined the secondary structure of BSA after interaction with synthetic chrysotile. The α -helix content was 30 ± 2% for the amide I region and 29 ± 2% for the amide III region. The content of β -sheet structure is 14 ± 3% for the amide I region and 13 ± 3% for the amide III region. In addition, the content of random structure is 22 ± 3% for the amide I region and 23 ± 2% for the amide III region. Finally, free BSA shows a β -turn content of 35 ± 2% for the amide I region and 34 ± 3% for the amide III region. Table 2 summarizes the percentages of secondary structures in lyophilized BSA before and after interaction with chrysotile, together with literature data for BSA in aqueous solution for comparison.^[38] Whereas the α -helix content is almost constant (about 30%), a significant decrease in the β -sheet content (from about 23% to about 14%) is found by comparing the free lyophilized BSA with the lyophilized BSA in the adduct. A significant increase in β -turn content, from about 20–24% to about 34%, and no variation in random structure are associated with the BSA–chrysotile interaction. The reduction in β -sheet content in the lyophilized BSA was also observed for the interaction of lyophilized BSA with poly(D,L-lactide-co-glycolide).^[27b,39]

The conformational transition resulting in a higher β -turn content was also observed for the interaction between BSA and different clay surfaces. In these cases, the increased effect of adsorption onto a charged surface rather than a neutral one emphasizes the importance of electrostatic interactions.^[40] Comparison with the protein secondary structure in solution suggests that the lyophilization process is associated mainly with a conformational transition from α -helix to

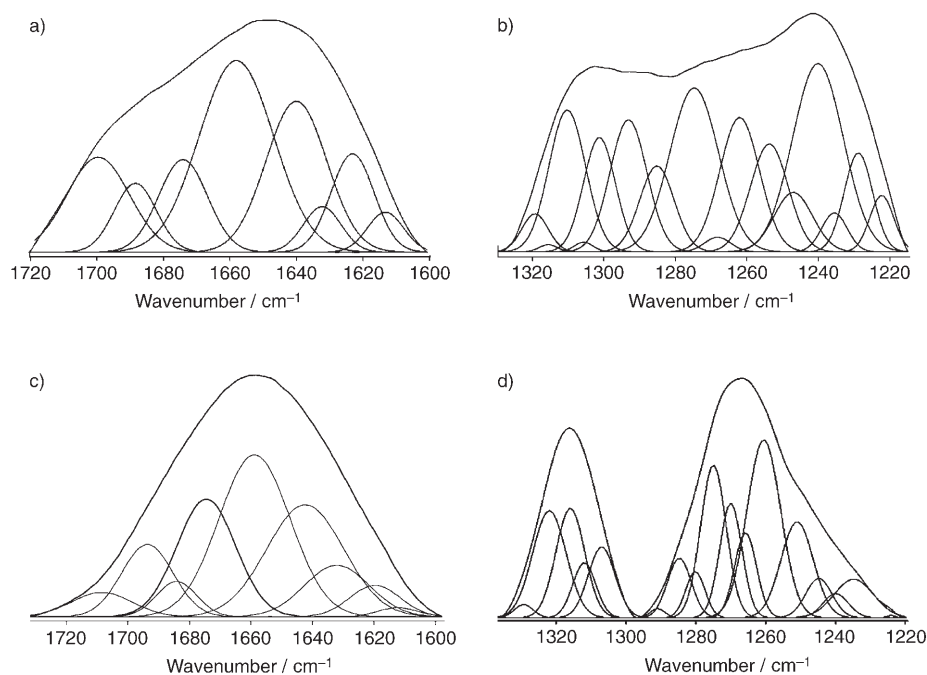


Figure 4. FTIR spectra and their Gaussian curve-fitting (the individual bands are shown underneath the IR spectra) obtained from ground samples (tens of micrograms) in KBr pellets of a) and b): lyophilized BSA, and c) and d): lyophilized synthetic chrysotile-BSA adduct. The spectra were collected within the ranges 1700–1600 and 1300–1220 cm^{-1} . Within these ranges the component bands of the protein vibration modes amide I and amide III, respectively, corresponding to different protein conformations, are shown. The IR absorbance is in arbitrary units.

Table 2. BSA secondary structure [%]. The \pm values are standard deviations calculated by analyzing three individual spectra in each case.

Sample	α -Helix [%]	β -Sheet [%]	Random [%]	β -Turn [%]
BSA lyophilized powder				
amide I	31 \pm 1	22 \pm 1	22 \pm 3	24 \pm 1
amide III	31 \pm 2	24 \pm 3	24 \pm 2	20 \pm 3
chrysotile-BSA adducts				
amide I	30 \pm 2	14 \pm 3	22 \pm 3	35 \pm 2
amide III	29 \pm 2	13 \pm 3	23 \pm 2	34 \pm 3
BSA in solution ^[37]	54 \pm 6	8 \pm 3		38 \pm 1

β -sheet, as previously reported,^[27b,39] whereas the formation of the adduct induces a transition to mainly β -turns. β -turns exhibit a much larger conformational variety than secondary structures constructed from periodic subunits, such as helices and β -sheets. β -turns consist predominantly of hydrophilic amino acid residues and are concentrated near the protein surface. As a consequence of the folded geometry of the protein backbone, the polar side-chain groups in corner positions point outward, and may be used as a site for molecular recognition.

The structural reorganization of the BSA, induced by the surface association with the chrysotile, is also supported by the FTIR spectra of the BSA and the chrysotile-BSA

adduct within the ranges 3000–2800 and 1440–1340 cm^{-1} , as shown in Figure 5a–d. In fact, we observe that in the adduct, the protein absorption bands at 2959 and 2871 cm^{-1} assigned to the CH_3 stretching decrease in intensity, whereas the bands at 2928 and 2854 cm^{-1} assigned to CH_2 stretching increase in intensity. The variation in absorption intensity of these stretching bands is consistent with the observed decrease in absorption intensity of the bending bands at 1455 cm^{-1} assigned to the CH_2 groups, and with the increase in absorption intensity of the bending bands at 1385 cm^{-1} assigned to the CH_3 groups.

Therefore, on the basis of the reported data, we can hypothesize that electrostatic interactions between the chrysotile surface and BSA induce a conformational change in the protein structure, with the formation of β -turns and a synergic reorganization of the chrysotile surface structure.

Conclusion

In this study, we used three different techniques (TEM, AFM, and FTIR) to demonstrate that both mineral and synthetic stoichiometric chrysotile fibers associate superficially with bovine serum albumin. Albumin was observed microscopically to adhere to the chrysotile fibers and could cover their entire surface. The physical interaction between chrysotile and albumin was allowed to occur at pH 7.4, at which point albumin and chrysotile are mainly negatively and positively charged, respectively.

The adsorption of albumin onto the chrysotile surface appears to be mainly electrostatically driven and stabilized by hydrogen bonds. The formation of the adduct induces clear modifications in BSA secondary structure, which were quantitatively evaluated. The protein undergoes a conformational transition to β -turns, which allows a better interaction among the protein hydrophilic side-chains and the charged mineral surface. In fact, the FTIR data obtained from the chrysotile-BSA adduct showed a modification of chrysotile absorption bands corresponding to outer Mg–OH vibration and inner Mg–O vibration, consistent with hydrogen-bonding interactions involving the superficial OH groups. Synthetic chrysotile nanocrystals that are adequately characterized, uniform in their properties, and devoid of foreign ions

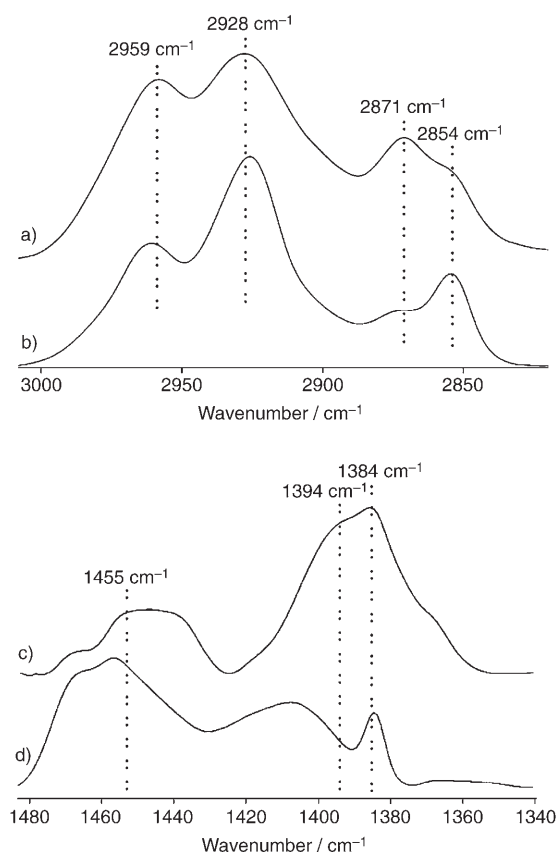


Figure 5. FTIR spectra obtained from ground samples (tens of micrograms) in KBr pellets of a) and c): lyophilized BSA, and b) and d): synthetic chrysotile-BSA adducts. The spectra were collected within the ranges 3000–2750 and 1400–1340 cm^{-1} . The IR absorbance is in arbitrary units.

have proven to be an ideal reference standard with which to study the interaction of chrysotile with biological systems, in order to elucidate the chemical mechanisms of asbestos toxicity.

Acknowledgement

This work was supported by MIUR and the University of Bologna (Funds for Selected Research Topics).

- [1] S. S. Chissick in *Encyclopedia of Physical Science and Technology* Vol. 2 (Ed.: R. A. Meyers), Academic Press, Orlando, **1987**, pp. 79–108.
- [2] B. A. Cressey, E. J. W. Whittaker, *Mineral. Mag.* **1993**, *57*, 729–732.
- [3] E. J. W. Whittaker, *Acta Crystallogr.* **1957**, *10*, 149–156.
- [4] K. Yada, K. Iishi, *Am. Mineral.* **1977**, *62*, 958–965.
- [5] D. S. O'Hanley, M. Dyar Darby, *Can. Mineral.* **1993**, *78*, 391–399.
- [6] F. J. Wiks, E. J. W. Whittaker, *Can. Mineral.* **1975**, *13*, 227–243.
- [7] G. Falini, E. Foresti, I. G. Lesci, N. Roveri, *Chem. Commun.* **2002**, 1512–1513.
- [8] G. Falini, E. Foresti, M. Gazzano, A. F. Gualtieri, M. Leoni, I. G. Lesci, N. Roveri, *Chem. Eur. J.* **2004**, *10*, 3043–3049.
- [9] B. T. Mossman, A. Churg, *Am. J. Respir. Crit. Care Med.* **1998**, *157*, 1666–1680.

- [10] B. Fubini, L. Mollo, E. Giamello, *Free Radical Res.* **1995**, *23*, 593–614.
- [11] C. Riganti, E. Aldieri, L. Bergandi, I. Fenoglio, C. Costamagna, B. Fubini, A. Bosia, D. Ghigo, *Free Radical Biol. Med.* **2002**, *32*, 938–949.
- [12] D. W. Kamp, V. Panduri, S. A. Weitzman, N. Chandel, *Mol. Cell. Biochem.* **2002**, *234–235*, 153–160.
- [13] D. R. Green, J. C. Reed, *Science* **1998**, *281*, 1309–1312.
- [14] J. Cai, D. P. Jones, *J. Biol. Chem.* **1998**, *273*, 11401–11404.
- [15] J. Jurinski, J. D. Rimstidt, *Am. Mineral.* **2001**, *86*, 392–399.
- [16] J. M. Davis, J. Addison, R. E. Bolton, K. Donaldson, A. D. Jones, T. Smith, *Br. J. Exp. Pathol.* **1986**, *67*, 415–430.
- [17] K. Miller, *Crit. Rev. Toxicol.* **1978**, *5*, 319–354.
- [18] F. Valerio, M. De Ferrari, L. Ottaggio, E. Repettò, L. Santi, *Mutat. Res.* **1980**, *122*, 397–402.
- [19] J. Wu, W. Liu, K. Koenig, S. Idell, V. C. Broaddus, *Am. J. Physiol.* **2000**, *279*, L916–923.
- [20] A. D. McLachlan, J. E. Walker, *J. Mol. Biol.* **1977**, *112*, 543–548.
- [21] J. R. Brown, P. Shockley in *Lipid-Protein Interactions Vol. 1* (Eds.: P. Jost, O. H. Griffith), Wiley, New York, **1982**, pp. 25–68.
- [22] X. M. He, D. C. Carter, *Nature* **1992**, *358*, 209–215.
- [23] S. Sugio, A. Kashima, S. Mochizuki, M. Noda, K. Kobayashi, *Protein Eng.* **1999**, 439–446.
- [24] T. Peters, Jr., *Adv. Protein Chem.* **1985**, *37*, 161–245.
- [25] J. X. Ho, E. W. Holowachuk, E. J. Norton, P. D. Twigg, D. C. Carter, *Eur. J. Biochem.* **1993**, *215*, 205–212.
- [26] N. Hagag, E. R. Birnbaum, D. W. Darnall, *Biochemistry* **1983**, *22*, 2420–2427.
- [27] a) K. Griebenow, A. M. Klibanov, *Proc. Natl. Acad. Sci. USA* **1995**, *92*, 10969–10975; b) K. G. Carrasquillo, A. M. Stanley, J. C. Aponte-Carro, P. De Jesus, H. R. Costantino, C. J. Bosques, K. Griebenow, *J. Controlled Release* **2001**, *76*, 199–208.
- [28] J. E. Morgan, A. J. Morgan, *Environ. Pollut.* **1998**, *99*, 167–175.
- [29] M. C. Jaurand, P. Baillif, J. H. Thomassin, L. Magne, J. C. Touray, *J. Colloid Interface Sci.* **1983**, *95*, 1–9.
- [30] R. Dumitru-Stanescu, C. Mandravel, C. Bercu, *Analyst* **1994**, *119*, 689–691.
- [31] S. Brunauer, P. H. Emmet, E. J. Teller, *J. Am. Chem. Soc.* **1938**, *60*, 309–319.
- [32] A. A. Hodgson in *Scientific Advances in Asbestos 1967–1985*, Anjalea Publications, Crowthorne, Berkshire, UK, **1986**, p. 186.
- [33] L. De Stefano, G. Buccolieri, *Ann. Chim.* **2001**, *91*, 277–283.
- [34] F. Valerio, D. Calducci, A. Lazzarotto, *Environ. Res.* **1987**, *44*, 312–320.
- [35] a) V. C. Farmer in *The Infrared Spectra of Minerals* (Ed.: V. C. Farmer), Mineral. Soc., London, **1974**, p. 331; b) C. J. Sernaand, B. D. Velde, *Mineral. Mag.* **1979**, *43*, 142–148.
- [36] a) E. Foresti, M. Gazzano, A. F. Gualtieri, I. G. Lesci, B. Lunelli, G. Pecchini, E. Renna, N. Roveri, *Anal. Bioanal. Chem.* **2003**, *376*, 653–658; b) J. T. Kloprogge, R. L. Frost, L. Rintoul, *Phys. Chem. Chem. Phys.* **1999**, *1*, 2559–2577; c) J. Min, X. Meng-Xia, Z. Dong, L. Yuan, L. Xiao-Chu, C. Xing, *J. Mol. Struct.* **2004**, *692*, 71–80; d) J. Kang, Y. Liu, X. Meng-Xia, S. Li, M. Jiang, Y.-D. Wang, *Biochim. Biophys. Acta* **2004**, *1674*, 205–214; e) T. Xu, R. Fu, L. Yan, *J. Colloid Interface Sci.* **2003**, *262*, 342–350.
- [37] R. J. Jakobsen, F. M. Wasacz, *Appl. Spectrosc.* **1990**, *44*, 1478–1489.
- [38] K. G. Carrasquillo, J. C. Aponte-Carro, A. Alejandro, D. Diaz Toro, K. Griebenow, *J. Pharm. Pharmacol.* **2001**, *53*, 115–120.
- [39] K. Fu, K. Griebenow, L. Hsieh, A. M. Klibanov, R. Langer, *J. Controlled Release* **1999**, *58*, 357–366.
- [40] S. Servagent-Noynville, M. Revault, H. Quiquampoix, M.-H. Baron, *J. Colloid Interface Sci.* **2000**, *221*, 273–283.
- [41] J. T. Pelton, L. R. McLean, *Anal. Biochem.* **2000**, *277*, 167–176.

Received: June 20, 2005
Published online: December 16, 2005